Lawrence Berkeley National Laboratory
LBL Publications

Title
Testing and demonstration of model predictive control applied to a radiant slab cooling
system in a building test facility

Permalink
https://escholarship.org/uc/item/0sq1h8hw

Authors
Pang, Xiufeng
Duarte, Carlos
Haves, Philip
et al.

Publication Date
2018-08-01

DOI
10.1016/j.enbuild.2018.05.013

Peer reviewed

Testing and demonstration of model predictive control applied to a radiant slab cooling system in a building test facility

Xiufeng Pang [a,*], Carlos Duarte [b], Philip Haves [a], Frank Chuang [c]

[a] Lawrence Berkeley National Laboratory, One Cyclotron Road, MS 90R3147, Berkeley, CA 94720, USA
[b] University of California-Berkeley, Berkeley, CA 94720, USA
[c] Tesla, Inc., Palo Alto, CA 94304, USA

ABSTRACT

Radiant slab systems have the potential to significantly reduce energy consumption in buildings. However, control of radiant slab systems is challenging. Classical feedback control is inadequate due to the large thermal inertia of the systems and heuristic feed-forward control often leads to unacceptable indoor comfort and may not achieve the full energy savings potential. Model predictive control (MPC) is now attracting increasing interest in the building industry and holds promise for radiant systems. However, an often-cited barrier to its implementation in the building industry is the high computational cost and complexity relative to the feedback controls used in conventional systems. The objectives of this study were to (i) verify the correct operation of an open source MPC toolchain developed for radiant slab systems, and (ii) demonstrate its efficacy in a test facility. A matched pair of cells in the FLEXLAB building test facility at the Lawrence Berkeley National Laboratory was used in the study. The proposed MPC toolchain was implemented in one cell and the performance compared to that of the other cell, which used a conventional heuristic control strategy. The results showed that the simplified MPC approach applied in the toolchain worked as expected and realized energy savings over the conventional control strategy. The MPC yielded 42% chilled water pump power reduction and 16% cooling thermal energy savings, while maintaining equal or better indoor comfort.

1. Introduction

Heating, ventilation, and air conditioning (HVAC) systems account for about 44% of the total energy use in U.S. buildings [1]. The energy consumption of HVAC systems has been shown to be sensitive to the quality of the control; enhanced control strategies can yield savings of 2%–16% [2] while incorrect control and other control-related faults can increase consumption by ~10%.[1]

Most HVAC systems found in buildings constructed after the 1980s use forced air systems, typically variable-air-volume (VAV) distribution systems [5] in North America. Forced air systems, or all-air systems, are designed to provide an indoor air heat balance to maintain occupant thermal comfort. These all-air systems can respond relatively quickly to changes in zone air temperatures due to the low thermal inertia of the air in the occupied space. Thus, conventional feedback controllers are generally adequate for this type of application.

Radiant heating and cooling systems meet 50% or more of the thermal load in the occupied space through long-wave radiant exchange. Radiant systems offer several advantages over typical all-air HVAC systems, enabling them to reduce HVAC energy consumption while maintaining equal or better occupant thermal comfort [6]. As a result, radiant systems are finding increasing application in high performance buildings [7], with over half of the zero net energy buildings in North America using radiant systems [8]. This current study is focused on hydronic radiant slab cooling systems, also called thermally activated building systems [9]. These systems use tubes embedded in the slab to circulate chilled water through the slab and use relatively large areas, typically the whole floor, ceiling, or both surfaces, for heat exchange, thereby reducing the temperature difference between the chilled water and the occupied space [9]. The advantages are:

- improved heat transport efficiency from the use of water rather than air,

---

* Corresponding author.
E-mail address: xpang@lbl.gov (X. Pang).

[1] A meta-study of commissioning identified 16% median actual savings from retro-commissioning [3], and a study of 481 operational issues identified in existing commercial buildings found that control problems accounted for >75% of the causes of energy waste [4].

- higher chilled water supply temperatures than are used in all-air systems, enabling greater use of water-side free cooling [10], and
- the ability to control the building's thermal mass for energy storage [11,12].

However, radiant slab systems are challenging to control due to their large thermal inertia. The time taken to respond to control signals is typically several hours or more [13], making feedback control of zone temperature infeasible. Any attempt to switchover quickly from heating to cooling or vice versa will result in wasted energy [14] and it is recommended that switchover time should be greater than 24 h [15,16]. The problem, in cooling mode, now becomes managing the heat extraction rate while considering the building's thermal mass within a single day to avoid both under- and over-cooling of the space during occupied hours. Although there is no clear consensus on a common control strategy, current control methods for radiant slab systems typically use heuristic feed-forward control, in which the supply water temperature or flow rate is based on ambient wet-bulb temperature, occupancy schedules or utility tariffs [17–19], or some combination thereof, to maintain a relatively constant slab temperature for all hours of the day. The advantage of this control strategy is that the peak cooling capacity of the plant system can be reduced since the heat extraction rate is spread over 24 h but it may not allow for active control of the thermal storage in the slab. Control of the thermal storage in the slab enables load shifting, in which the load profile of the HVAC system is manipulated for the building stakeholders' benefit. The operation of the HVAC system can be shifted to nighttime hours where favorable weather conditions and electricity prices exist [20]. The ability of the HVAC system to shift load also enables a large fraction of the load of the building to participate in utility demand response programs, which aim to stabilize power grids [21].

The radiant slab research community has been actively developing control strategies, with the aim of exploiting the advantages of radiant slab cooling systems discussed above. A major effort has been undertaken in model predictive control (MPC) [19,22]. Model predictive control (MPC) is an advanced control method that is now attracting increasing interest in the buildings industry [23–25]. MPC can use forecasts of weather [26], occupancy, and energy price signals [27,12,28] to manage thermal energy storage, e.g. in radiant slabs, to improve occupant thermal comfort and reduce energy consumption and costs [12,23]. In MPC, an optimization problem is solved on-line to obtain the current control action [29]. MPC returns a sequence of optimal control actions based on the current state and dynamic model of the plant, system constraints, and minimization of a cost function; only the first control action of the sequence is applied and the procedure is repeated at predetermined intervals. An often cited barrier to its implementation in the building industry is its high computational cost and complexity. In this study, it was shown that with the proper model structure, the model can be identified and is accurate enough to implement real time control and realize energy savings over conventional controllers and the process can be simplified through the use of an open source MPC toolchain.

The main contributions of this experimental study are the demonstration of a MPC model structure for radiant slab cooling systems that can be easily identified, robust, and accurate enough to be used for real-time control and the direct comparison of MPC to heuristic control based on a fixed operational schedule using a matched pair of test cells.

The rest of the paper is organized as follows. Section 2.1 describes the MPC controller used in this study with more detail. Sections 2.2–2.4 describes the test facility, measurement instrumentation, and experimental setup used to carry out this study.

Sections 3 and 4 gives the experiment results and concluding remarks, respectively.

2. Methodology

2.1. MPC controller

The MPC controller has the goal of determining a binary control output (ON/OFF) of the radiant slab system that minimizes the weighted combination of comfort violations and energy consumption over a prediction horizon of N time steps. The control problem is defined in Eq. (1) [31].

$$\min_{c_k, h_k} \sum_{k=t}^{t+N} \left[\rho \max\{x_{z,k} - x_{\max,k}, 0, x_{\min,k} - x_{z,k}\} + c_k + h_k \right]$$

$$subject\ to\ x_{k+1}$$

$$= \begin{cases} A_{cool}x_k + W_{cool}d_k & if\ c_k = 1,\ h_k = 0 \\ A_{heat}x_k + W_{heat}d_k & if\ c_k = 0,\ h_k = 1 \\ A_{coast}x_k + W_{coast}d_k & if\ c_k = 0,\ h_k = 0 \end{cases} \quad \forall k \in \{t, \dots, t+N-1\} \quad (1)$$

where $x_k = [x_{slab,k} \quad x_{z,k}]'$ and $d_k = [d_{sol,k} \quad d_{oat,k} \quad d_{hg,k}]'$ are the state and disturbance vectors, respectively, $x_{slab,k}$ is slab temperature [°C], $x_{z,k}$ is zone operative temperature [°C], $d_{sol,k}$ is solar irradiance [W/m^2], $d_{oat,k}$ is outdoor dry-bulb air temperature [°C], $d_{hg,k}$ is the sum of the heat gains from the lights, miscellaneous loads and occupants [W], $x_{\max,k}$ and $x_{\min,k}$ are the maximum and minimum bounds for the zone operative temperature [°C], c_k and h_k are indicator variables for the cold and hot water valves, respectively, and ρ is the weight to adjust between comfort satisfaction and energy consumption. The subscript t indicates the actual time when the optimization takes place while k indicates the future predictions beyond time t.

The optimization problem in (1) can be equivalently formulated as a mixed-integer linear program; the steps are described briefly below. The reader is referred to Borrelli et al. [32] for a more in-depth discussion of MPC and hybrid system modeling. The temperature violation cost in (1) is formulated as a maximum of three linear pieces. This cost term is transformed into a linear program by means of slack variables. At each time step, a slack variable is introduced and set greater than or equal to the three linear pieces at that time step. The temperature violation cost then becomes the sum of the slack variables. Next, the switched system dynamics can be formulated in simplified form as follows for each time step k.

$$x_{k+1} = z_1 + z_2 + A_{coast}x_k + W_{coast}d_k \quad (2a)$$

$$z_1 = \begin{cases} A_{cool}x_k + W_{cool}d_k - A_{coast}x_k - W_{coast}d_k & if\ c_k = 1 \\ 0 & if\ c_k = 0 \end{cases} \quad (2b)$$

$$z_2 = \begin{cases} A_{heat}x_k + W_{heat}d_k - A_{coast}x_k - W_{coast}d_k & if\ h_k = 1 \\ 0 & if\ h_k = 0 \end{cases} \quad (2c)$$

$$c_k + h_k \leq 1 \quad (2d)$$

The remaining switched dynamics are then reformulated as mixed-integer linear constraints as follows.

$$-M_1 c_k + z_1 \leq A_{cool}x_k + W_{cool}d_k - A_{coast}x_k - W_{coast}d_k \quad (3a)$$

$$m_1 c_k - z_1 \leq -A_{cool}x_k - W_{cool}d_k + A_{coast}x_k + W_{coast}d_k \quad (3b)$$

$$m_1(1 - c_k) + z_1 \leq 0 \quad (3c)$$
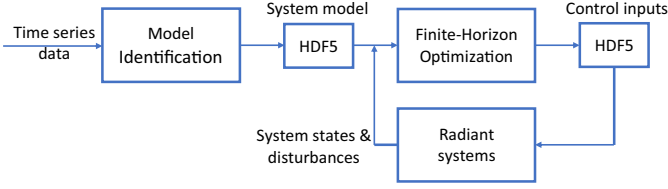
$$-M_1(1 - c_k) - z_1 \leq 0 \quad (3d)$$

Fig. 1. System diagram of the MPC toolchain.

$$-M_2 h_k + z_2 \leq A_{heat} x_k + W_{heat} d_k - A_{coast} x_k - W_{coast} d_k \quad (3e)$$

$$m_2 h_k - z_2 \leq -A_{heat} x_k - W_{heat} d_k + A_{coast} x_k + W_{coast} d_k \quad (3f)$$

$$m_2(1 - h_k) + z_2 \leq 0 \quad (3g)$$

$$-M_2(1 - h_k) - z_2 \leq 0 \quad (3h)$$

where

$$M_1 = \max(A_{cool} x_k - W_{cool} d_k - A_{coast} x_k + W_{coast} d_k)$$

$$m_1 = \min(A_{cool} x_k - W_{cool} d_k - A_{coast} x_k + W_{coast} d_k)$$

$$M_2 = \max(A_{heat} x_k - W_{heat} d_k - A_{coast} x_k + W_{coast} d_k)$$

$$m_2 = \min(A_{heat} x_k - W_{heat} d_k - A_{coast} x_k + W_{coast} d_k).$$

This is sometimes referred to as the big-M formulation of the switched affine system.

In Feng et al [30], a similar MPC formulation was implemented in MATLAB. The modeling language YALMIP was used to formulate the mixed-integer linear program and the commercial solver Gurobi was used to solve the problem. Unfortunately, the software toolchain was accessible only to users with academic or paid commercial licenses. In order to make the software more freely available and transparent to users, it was decided to rewrite the toolchain using only open-sourced software.

In the current implementation, Julia has replaced MATLAB as the programming language while COIN−OR Branch and Cut (CBC) has replaced Gurobi as the mixed-integer solver. Julia offers an optimization modeling language, named JuMP, as part of its optimization package JuliaOpt. JuliaOpt also includes the necessary modules to interface with third-party solvers such as CBC. The optimization problem was modeled using JuMP but reformulated using the big-M method to express the switched-system dynamics (this was unnecessary in YALMIP since YALMIP allowed for logical constraint switching). The JuMP formulation is then passed to CBC using the JuliaOpt interface. CBC, while slower than Gurobi for larger problems, solves the problem in reasonable time given the control sampling interval (1 hour). All system dynamics and optimization solution data are saved using the HDF5 data format. HDF5 is a fast and space-efficient way to store and transfer data and has interfaces for most popular language, such as Python, MATLAB, Julia and C/C++. This ensures that there is a reliable way for cross-platform software to access the information generated by the Julia code.

The MPC toolchain consists of two main modules, model identification and control optimization. The system diagram is shown in Fig. 1. The model identification module receives time-series system response data from the radiant slab system concerned to identify a simplified, switched-system model. The module solves a nonlinear least squares optimization problem to fit the model parameters A_{cool}, A_{heat}, A_{coast}, W_{cool}, W_{heat} and W_{coast} to the data. The model parameters are saved in HDF5 file format to be accessed by other modules.

The finite-horizon optimization module reads the system model parameters from the HDF5 file as well as the current system state variables and disturbances passed in from the radiant system concerned as function arguments. The optimization module then solves the energy cost minimization problem defined in Eq. (1) to arrive at the control inputs to the radiant system concerned to apply at the current time. The control inputs are also stored in HDF5 format for later access.

2.2. Test facility

The experiments were carried out in the Facility for Low Energy eXperiments (FLEXLAB [33]) at the Lawrence Berkeley National Laboratory (LBNL). FLEXLAB has four test beds, as shown in Fig. 2, and each test bed consists of two side-by-side cells with the same dimensions and construction. The thermal isolation resulting from the near adiabatic walls between adjacent cells allows their performance to be analyzed independently. The test bed used in this study consists of a pair of matched cells (1A and 1B, shown in Fig. 2), each is $9.14\,\text{m} \times 6.09\,\text{m} \times 4.88\,\text{m}$ with a floor area of 56 m^2 and has PEX tubing embedded in a dense concrete topping slab 100 mm thick. The two cells share a chiller and boiler plant and each cell has dedicated secondary loops for chilled water and hot water as shown in Fig. 3. The secondary chilled water and hot water supply temperature can be maintained at desired set points by mixing the supply and return water using a three-way modulating valve. The water temperatures and flow rates of both the primary and secondary loops were measured. The conventional control scenario was implemented in Cell 1A and the MPC was implemented in Cell 1B In this study, the focus was on the cooling performance.

The radiant slab system inside the cell is shown in Fig. 4. Hot water or chilled water is selected using automated control valves with manual overrides. The radiant slab system is divided into four sub-systems, each containing multiple circuits of PEX tubing, serving floor areas of 19.5 m^2, 9.6 m^2, 5.8 m^2 and 21.1 m^2, respectively. The nominal diameter of the tubing is 15.9 mm, and the internal diameter is 12.7 mm, with a tube spacing of 0.23 m on center.

Single-pane clear windows are used on the south façades of the two cells and the window area is 10.76 m^2 (5.88 m (L) × 1.83 m (H)).

In order to simulate a typical office, workspaces consisting of thermal manikins, desks and partitions were set up, together with artificial lights, as shown in Fig. 5. The manikins were wound with heating tape and the supply voltage adjusted to produce sensible heat dissipation rates of ∼80 W each, corresponding to the metabolic rate of sedentary office workers in a low humidity environment. The advantage of the thermal manikins is that their radiative/convective splits, and the characteristics of their thermal plumes, are more realistic than the heated cylinders specified in the European Standard E 14240. The total overhead lighting power is ∼180 W in each cell. Ping pong ball sensors were used to measure the operative temperature in both cells.

2.3. Instrumentation

FLEXLAB is well instrumented with research-grade sensors and meters. The most relevant measurements in the experiments reported here are listed in Table 1.

The room operative temperature was approximated by the average of the readings of three grey-painted ping-pong ball globe thermometers, as shown in Fig. 5. Humphreys reported that for low air velocity (<0.15 m/s), a 40 mm diameter globe has radiative and convective losses in the same ratio as the human body [34]. The three ping-pong ball sensors were placed on desks near the
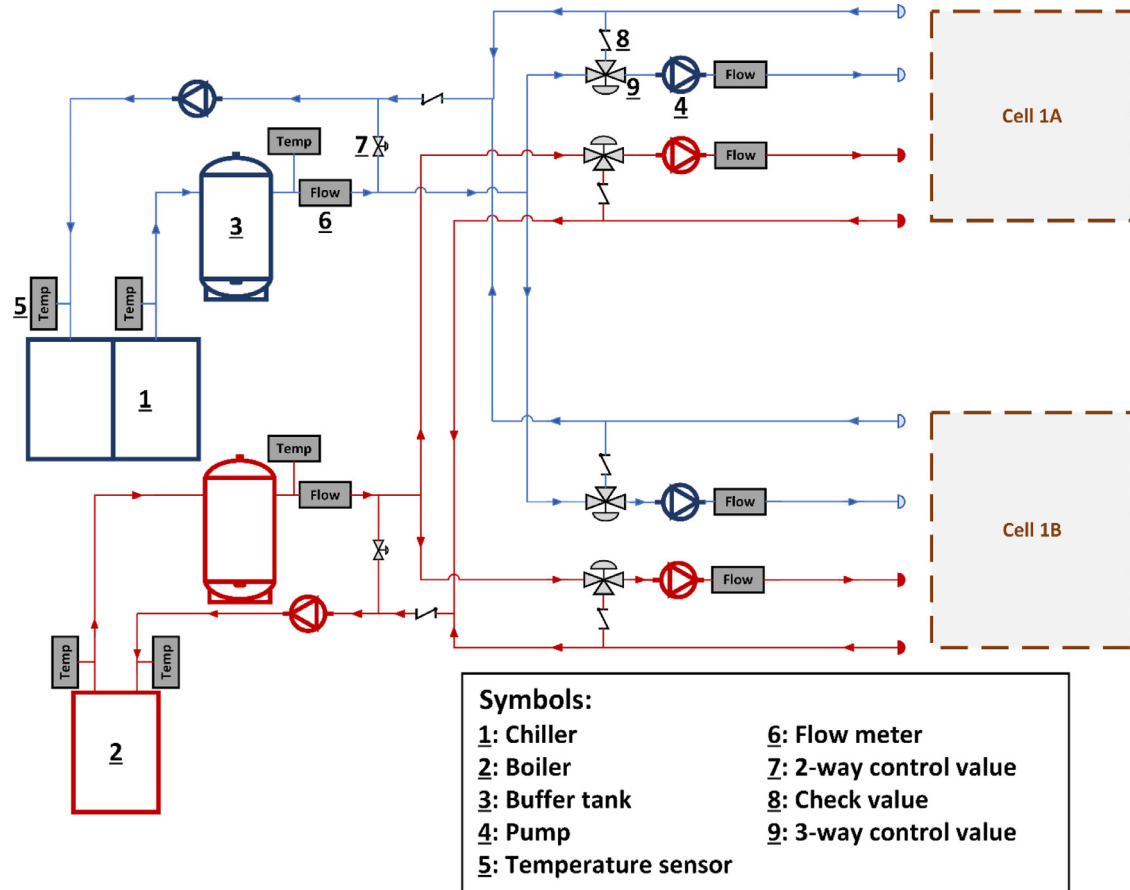
Fig. 2. General view of the test facility.

Symbols:
1: Chiller   **6: Flow meter**
2: Boiler   **7: 2-way control value**
3: Buffer tank   **8: Check value**
4: Pump   **9: 3-way control value**
5: Temperature sensor

Fig. 3. Schematic diagram of the chilled and hot water plant.

Table 1
Measurements in the experiment along with the accuracy ratings.

Measurement	Accuracy
Room operative temperature	±0.2 K
Radiant slab water flow rate	±1%
Radiant slab chilled water supply and return temperature	±0.1 K
Slab temperature	±0.1 K
Global horizontal irradiance	±5% or ±10 W/m^2
Circulation pump power	±2% of reading
Total lighting power	±1% of reading
Total manikin power	±1% of reading

window, in the middle of the cell and at the back of the cell respectively.

The slab temperatures were measured by three immersion-type sensors installed in thermowells that are about 13 mm below the surface, along the cell's North-South center line. The sensors are at 1.8 m, 4.6 m and 7.6 m from the south wall (the window) and are positioned halfway between adjacent tubes. The average of the readings from these three sensors was used to represent the temperature of the slab.

2.4. Experiment

2.4.1. Preparation

The seven circuits of the radiant slab system in each cell were balanced to ensure an even distribution of water flow rate in each circuit. The secondary chilled water pump speeds were adjusted to supply 26.5 lpm of water to each radiant slab system and each circuit had a flow rate of 3.8 lpm. The chilled water supply temperature was fixed at 11 °C.
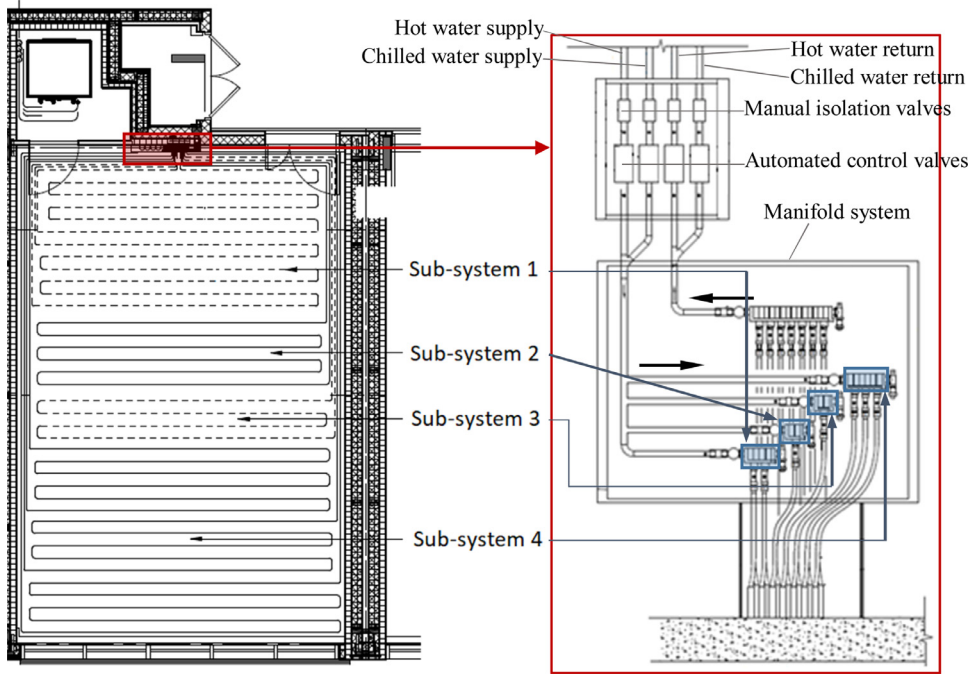
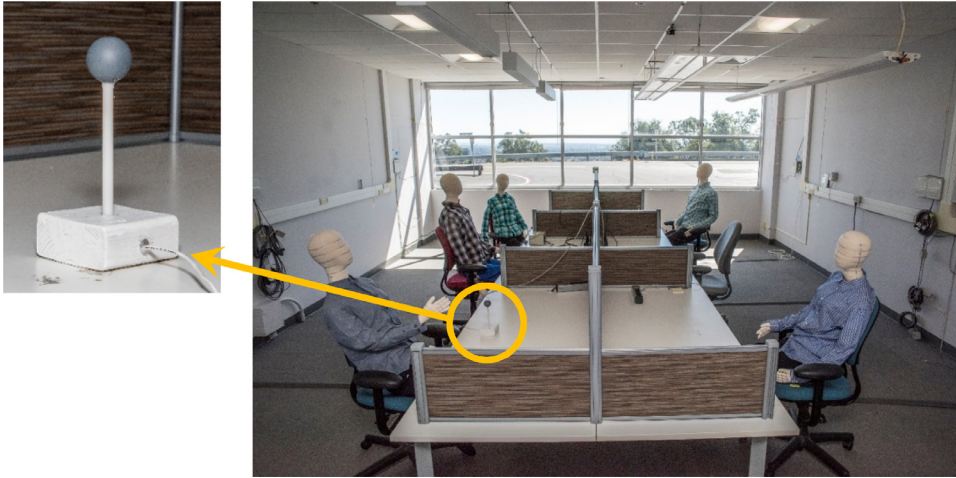**Fig. 4.** Radiant slab manifold system diagram.

Fig. 5. Test cell setup.

The manikins and lights of both cells were controlled by digital plug-in timers and programmed to be on from 8 am to 6 pm. The average internal load in Cell 1A was 571.7 W (391.5 W from manikins and 180.2 W from lights) and 600.7 W in Cell 1B (424.8 W from manikins and 175.9 W from lights). The internal heat gain in 1B (running the MPC) was ~5% greater than the internal heat gain in 1A.

FLEXLAB uses a customized control system that has a Python interface to execute control commands and access its database. The Simple Measuring and Actuation Profile (sMAP) [35] developed at the University of California, Berkeley, is used for data archiving. All automated control devices had been tested and calibrated for proper operation.

2.4.2. Validation of MPC toolchain

Validation of the MPC toolchain involved testing of the model identification module and the finite-horizon optimization module, shown in Fig. 1. The computer that ran the MPC toolchain used 64-bit Ubuntu 16.04 as the operating system and had an i7-860 2.80 GHz quad core processor.

The process used to validate the model identification module is shown in Fig. 6. A Python script was developed to execute step-tests of the radiant system in Cell 1B to produce time series data for model identification. The data were stored in sMAP and then exported manually to a csv file, which was then passed to the model identification module where the model parameters were identified and saved in HDF5 file format. Lastly, the identified model took inputs from the time series data and computed predictions. The model identification module is considered validated if the model parameters are successfully identified and the resulting model can predict the radiant system performance reasonably well and meet the following criteria: a Coefficient of Variation of the Root-Mean-Square Error (CV[$RMSE$]) < 10% and a Normalized Mean Bias Error (NMBE) < 5% [36].

$$CV(RMSE) = \frac{\sqrt{\frac{\sum_{i=1}^{n}(y_i - \hat{y}_i)^2}{n-1}}}{\bar{y}} \qquad (4)$$

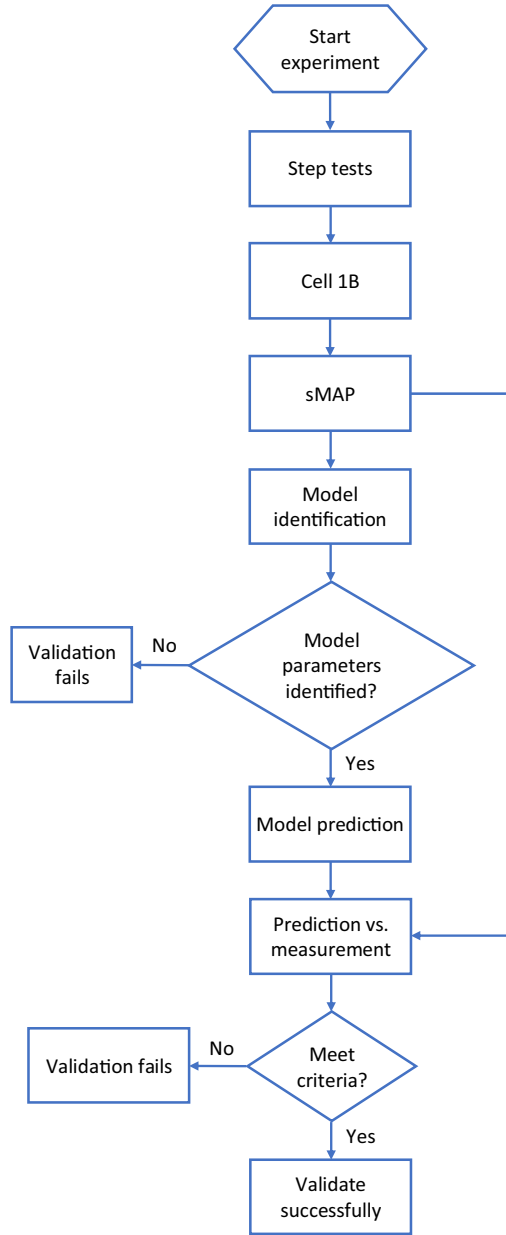$$NMBE = \frac{\sum_{i=1}^{n}(y_i - \hat{y}_i)}{(n-1) \times \bar{y}} \qquad (5)$$

Fig. 6. Procedure for testing and validating the model identification module.

where,

y_i = measured hourly data,
$\hat{y}_i$ = model predicted hourly data,
$\bar{y}$ = average measured data,
n = number of data points.

Once the model identification module had been validated, validation of the finite-horizon optimization module followed, as shown in Fig. 7. Radiant slab radiant systems have large time constants, with the response time of the surface temperature to a control input being several hours [14]. In this study, the control horizon, N, had been empirically set to 12 h, and the optimization problem run every hour, using a time-step of one hour. At each time step, only the control at the current time was applied. New values of the state variables and disturbances were sampled at each time-step and the cycle repeated.

The outside air temperature and sky cover forecast data were obtained from the U.S. National Weather Service website [37]. The
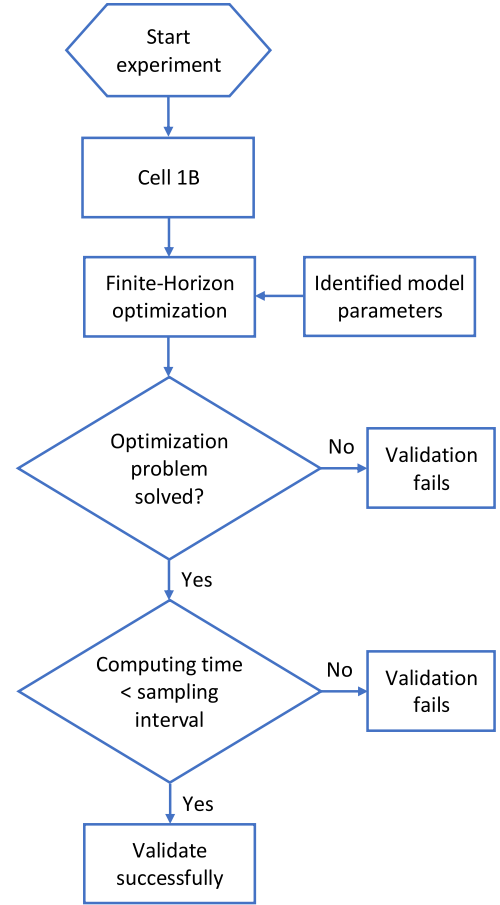

Fig. 7. Procedure for testing and validating the optimization module.

forecast global horizontal irradiance values on each day were determined using historical data measured at FLEXLAB on a day a year previously for which the forecast sky cover profile was closely similar. For example, the forecast of global horizontal irradiance on Oct 11th, 2017 consisted of hourly data measured on Oct 6th, 2016, the sky cover profile on Oct 6th, 2016 being closely similar to the forecast sky cover on Oct 11th, 2017.

A Python script was developed to obtain the state variables, i.e. the slab temperature and the zone operative temperature, and the disturbances, i.e. the solar irradiance, the outdoor air temperature and the internal heat gains, from the FLEXLAB data acquisition system and pass them to the finite-horizon optimization module at each time step. Using the identified model parameters, the finite-horizon optimization module solves the optimization problem defined in Eq. (1). The finite-horizon optimization module is considered validated if a solution is presented and the computing time is less than the time step.

2.4.3. MPC vs. heuristic control comparison

After the MPC toolchain was validated, its effectiveness was evaluated by comparing its performance to that of a heuristic control strategy that turns the radiant slab system on three hours prior to occupancy and turns it off one hour before occupancy ends. A typical office building occupancy schedule of 8:00 to 18:00 was used and the internal loads (the manikins and the lights) were enabled/disabled on the same schedule. Soft constraints and no hard constraints were imposed on the operative temperature. x_{max} and x_{min} were set to 26 °C and 19 °C, respectively, for hours between 7:00 and 17:00 and 47 °C and 10 °C for all other hours. No constraints were imposed on the slab temperature but some is-
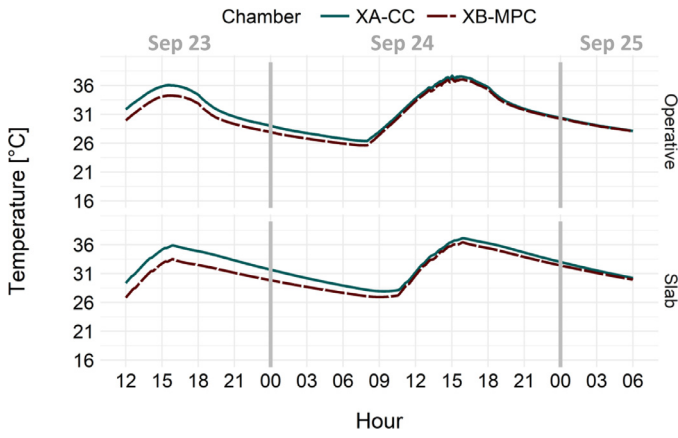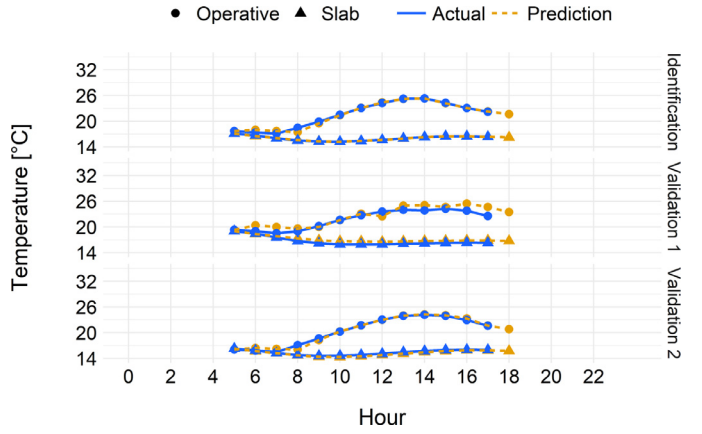
Fig. 8. Internal conditions in the "free response" mode.

Fig. 9. Internal conditions in the "radiant slab activated" mode.

Fig. 10. "Radiant slab activated" model identification and validation.

sues to consider in practice are condensation on the slab surface and thermal discomfort that may arise from the close contact of occupant's feet with a cold surface. Various values of the variable ρ were tested and a value of 100 was found to yield a reasonable trade-off between energy use and thermal discomfort, based on engineering judgment. Python scripts were developed to read the control signals from the HDF5 file, send them to the FLEXLAB and return the system outputs to the optimization block.

Before the MPC vs. heuristic control experiment, it was necessary to compare Cell 1A and Cell 1B in the "free response" and the "radiant slab activated" modes side by side to assess how closely the two cells matched each other and ensure the two cells start off at the similar initial conditions for the MPC vs. heuristic control experiment. In the "free response" mode, there is no mechanical cooling or heating and the changes in the interior conditions are the results of the weather and internal gain disturbances, whereas in the "radiant slab activated" mode, the radiant slab systems in both cells are activated with the chilled water flow rate at 26.5 lpm and the chilled water temperature at ~11 °C.

The "free response" experiment took place during Sep 23 – 25, 2017, and the "radiant slab activated" experiment took place during Sep 27 – 29, 2017. The results were shown in Figs. 8 and 9 respectively. In the "free response" experiment, Cell 1A started off with the operative temperature at 31.86 °C and the slab temperature at 29.35 °C, and Cell 1B started off with the operative temperature at 29.94 °C and the slab temperature at 26.82 °C, at noon. The differences between the initial operative temperatures and between the slab temperatures were 1.92 K and 2.53 K respectively. In the "radiant slab activated" experiment, Cell 1A started off with the opera-

tive temperature at 37.19 °C and the slab temperature at 32.80 °C, and Cell 1B started off with the operative temperature at 34.42 °C and the slab temperature at 28.62 °C. The differences between the initial operative temperatures and between the slab temperature were 2.77 K and 4.18 K, respectively. It took about 42 h for the "free response" and 36 h for the "radiant slab activated" to reach static states. As can be seen from Figs. 8 and 9, the two cells matched each other well in both the "free response" mode and the "radiant slab activated" mode. The average difference of the operative temperatures was 0.11 K and of the slab temperatures was 0.19 K in the "free response" mode and 0.16 K and 0.03 K, respectively, in the "radiant slab activated" mode.

3. Results and discussions

3.1. Validation of MPC toolchain

As the study focused on the cooling performance, the switched discrete model, described in Eq. (1), could only select the modes cooling or coasting; thus, only the model parameters for the two modes needed to be identified. Step-tests were performed to identify model parameters A_{cool}, A_{coast}, W_{cool}, and W_{coast}. The step-tests were run to collect two datasets of 12 hours in the cooling mode in which a step change of the chilled water flow from 0 to 26.5 lpm was executed with the manikins and the lights operating on the schedule from 8:00 to 18:00. State and disturbance variables, i.e. the room operative temperature, the slab temperature, the manikins and lighting power, the outside air temperature, and the global horizontal irradiance, were monitored at one-hour intervals. One 12 h dataset was used to identify the model parameters and the other to validate them. The same procedure was used for the coasting model parameter, with two datasets of 24 h. The model parameters were successfully identified and the comparison between the predictions and the measurements is presented below.

Fig. 10 presents the results of the cooling mode model identification and validation. Two datasets were used to validate the robustness of the identified model with different disturbances. The top chart shows the model prediction vs. the actual measurement using the same dataset for the model identification. The middle and bottom charts show the model prediction vs. actual measurement using different datasets. The data used in the bottom chart (Validation 2) were generated using similar disturbances as the training data, while the data in the middle chart (Validation 1) was generated with disturbances that were considerably different from the training data, as shown in Fig. 11. The slab temperature showed
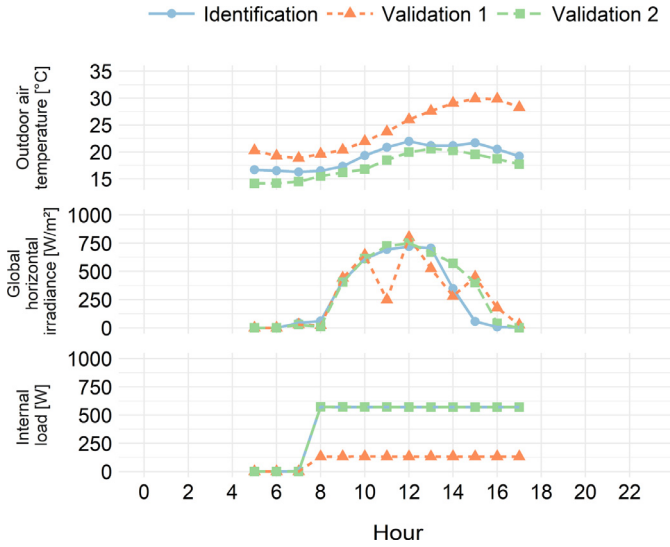
Fig. 11. Disturbances of the identification and validation datasets.
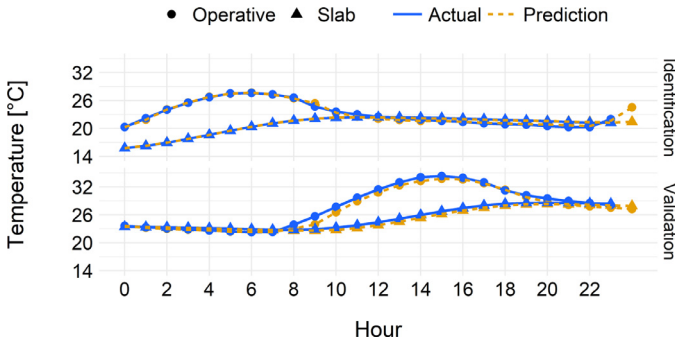

Fig. 12. "Free response" model identification and validation.
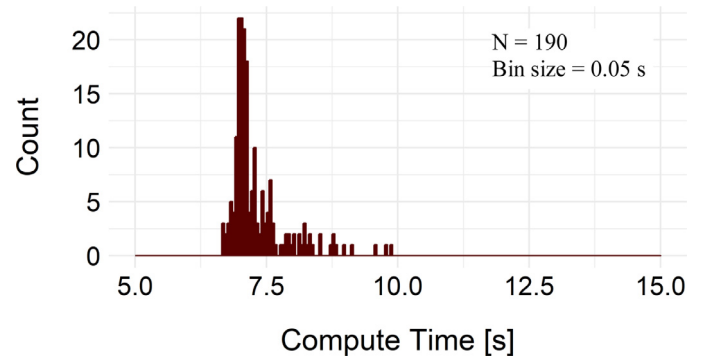

Fig. 13. Distribution of computation time for solving the MPC problem.

Table 2
CV(RMSE) and NMBE of the validation dataset.

Operation	Dataset	Variable	CV(RMSE)	NMBE
Cooling	Validation 1	Operative temperature	5.2%	−3.4%
Cooling	Validation 1	Slab temperature	3.4%	−3.2%
Cooling	Validation 2	Operative temperature	2.1%	−0.2%
Cooling	Validation 2	Slab temperature	1.5%	1.4%
Coasting	Validation	Operative temperature	2.4%	1.7%
Coasting	Validation	Slab temperature	1.5%	1.2%

Table 2 shows the CV(RMSE) and NMBE of the validation datasets. The two coefficients are both well below the 10% for CV(RMSE) and 5% for NMBE requirements.

The Finite-Horizon Optimization module was also validated successfully. Optimal solutions were presented at each time step during the validation period of 24 h. Fig. 13 shows the distribution of the computation time to solve the MPC problem. The computing time for each time step varied from 6.68 to 9.87 s with a mean of 7.33 s. Fig. 14 shows a snapshot of its running status.

3.2. MPC vs. heuristic control

Side-by-side measurements were made for a period of eight days, starting on Oct 11th, 2017. The internal loads were reduced by ~75% to emulate low load conditions from Oct 16th to Oct 18th. The results were shown in Figs. 15–17. The comparison focuses on the room operative temperature and the energy performance. As the two cells share the same chiller, there is no direct measurement of the chiller electricity consumption of each case. The cool-

less deviation than the room operative temperature. The maximum room operative temperature error was ±1.8 °C.

Fig. 12 shows the results of the coasting mode model identification and validation. The model identified for the coasting mode has better performance than the cooling mode, and the maximum operative temperature error is within ±1.0 °C.


```
Solve time is 7.28548897
[0.0 1.0 1.0 1.0 1.0 1.0 1.0 1.0 0.0 0.0 0.0 0.0; 1.0 0.0 0.0 0.0 0.0 0.0 0.0 0.0 1.0 1.0 1.0 1.0]

Output is 0.0
States are: [17.15 17.3528 16.8975 16.574 16.4992 16.6259 16.8552 17.1265 17.3914 18.3129 19.1039 19.74
28 20.149; 19.92 18.0799 19.6762 20.6301 22.8469 24.2659 25.5484 26.1497 26.2803 26.0613 25.7159 24.764
5 22.2138]

Slacks are: [0.0; 0.920094; 0.0; 0.0; 0.0; 0.0; 0.0; 0.149685; 0.28031; 0.0612956; 0.0; 0.0]

Sum of modes are: 6.999999999999999

Sum of slacks: 1.411384199079061

Used upper setpoints: [26.0,26.0,26.0,26.0,26.0,26.0,26.0,26.0,26.0,26.0,26.0,47.0]

Used lower setpoints: [19.0,19.0,19.0,19.0,19.0,19.0,19.0,19.0,19.0,19.0,19.0,10.0]

Cost is : 148.13841990322146
```

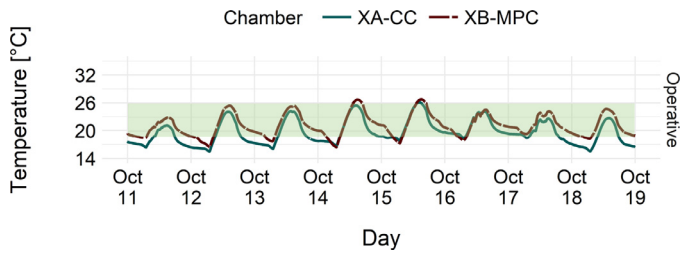**Fig. 14.** Snapshot of Finite-Horizon Optimization running status.

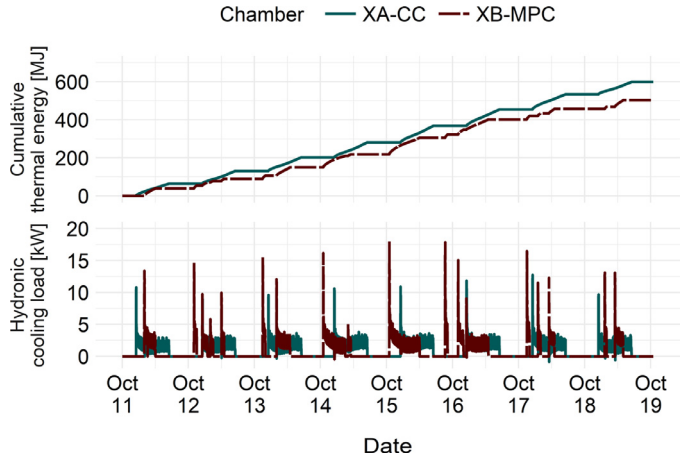**Fig. 15.** Comparison of the average room operative temperature.

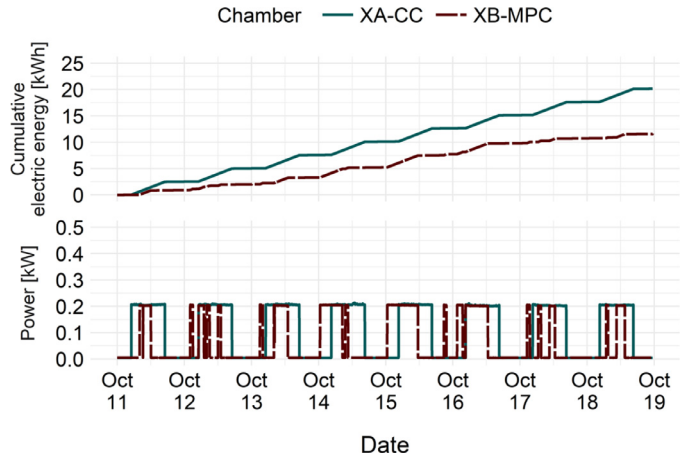**Fig. 16.** Comparison of the rate of thermal energy consumption.

Fig. 17. Comparison of the pump power consumption and the corresponding energy consumption.

ing thermal energy, calculated as the product of the chilled water capacity rate and the difference between the chilled water supply and return temperatures of the radiant slab system, was used as a proxy for the chiller electricity consumption. The energy performance consists of two components, the cooling thermal energy and the chilled water pumping energy.

Fig. 15 compares the room operative temperature. As can be seen from the figure, most of the time, the room operative temperatures in both cases were maintained within the set-point range from 19 °C to 26 °C (indicated by the shade area) during the occupied hours of 8:00–18:00. The exceptions mainly occurred in the early morning where the room operative temperatures in both cases were lower than 19 °C and the performance of the heuristic control is worse than that of the MPC. This behavior is an inherent characteristic of radiant slab systems as they rely on the thermal

mass of the slab to store sufficient cooling capacity in the early morning. However, with carefully selected value of the variable ρ, a trade-off between energy use and the thermal discomfort can be achieved to reduce overcooling in the early morning. On Oct 14th and 15th, the high outside air temperature and clear sky resulted in an increased cooling load which approached the cooling capacity of the radiant slab system in both cells, and thus the room operative temperature in both cells were slightly higher than 26 °C.

Fig. 16 compares the rate of consumption of thermal energy while Fig. 17 compares the pump power consumption. The upper chart shows the cumulative value and the lower chart shows the instant measurement. The cumulative thermal energy consumption using the MPC was 503.0 MJ and was 598.9 MJ using heuristic control, yielding a thermal energy saving of 16.0% during the eight days of the experimental period, which indicates a 16.0% chiller electricity savings from the MPC. The cumulative chilled water pump electricity consumption with the MPC was 11.6 kWh and with the heuristic control was 20.2 kWh, yielding an electricity saving of 42.6%. The savings are more substantial when the system operates at partial load conditions, i.e. when the room cooling load is smaller than the cooling capacity of the radiant slab. When the room cooling load approaches the cooling capacity of the radiant slab, the benefit of MPC diminishes. As can be seen from the data on Oct 15th, the MPC only shifted the operating hours of the pump and the total pump running time was just one hour less than that with the conventional control.

4. Conclusions

The open source MPC toolchain was tested and validated in the FLEXLEB test facility. The identified model reasonably represented the performance of the radiant slab system with a CV(RMSE) less than 10% and a NMBE less than 5%. The Finite-Horizon Optimization module successfully solved the optimization problem and the average computing time was 7.33 s per zone for a one hour time-step. In order for the computation time to be small compared to the time-step in a large building, which could have 100–1,000 zones, some form of parallel processing would be required, possibly using a graphics card; further investigation is required.

During the eight day experimental period, the MPC yielded 42.6% chilled water pumping energy reduction and 16.0% cooling thermal energy savings when compared to the conventional control of the radiant slab system, while maintaining equal or better indoor comfort.

The MPC toolchain needs to perform step tests of the radiant slab system to collect data for model identification. The data can be obtained actively or passively depending on the actual conditions. The passive approach is preferred as the normal operation of the radiant system would not be interrupted. This is essential for the MPC toolchain to be widely accepted and applied in the HVAC industry. Therefore, future research is needed to investigate how the data collected passively would impact the model accuracy and how model accuracy would impact the performance of the MPC toolchain.

References

[1] EIA, Commercial Building Energy Consumption Survey (CBECS), 2012. http://www.eia.gov/tools/faqs/faq.cfm?id=86&t=1, (accessed February 26, 2015).

[2] S. Wang, Z. Ma, Supervisory and optimal control of building HVAC systems: a review, HVACR Res. 14 (2008) 3–32, doi:10.1080/10789669.2008.10390991.

[3] E. Mills, Building commissioning: a golden opportunity for reducing energy costs and greenhouse-gas emissions, 2009. doi:10.2172/985240.

[4] J. Effinger, H. Friedman, C. Morales, E. Sibley, S. Tingey, A Study on Energy Savings and Measure Cost Effectiveness of Existing Building Commissioning, IEA Annex 47 (2009).

[5] D.W. Winiarski, W. Jiang, M.A. Halverson, Review of Pre-and Post-1980 Buildings in CBECS–HVAC Equipment, Pacific Northwest National Laboratory, Richland, WA, 2006 http://www.pnl.gov/main/publications/external/technical_reports/PNNL-20346.pdf accessed April 27, 2016.

[6] C. Karmann, S. Schiavon, F. Bauman, Thermal comfort in buildings using radiant vs. all-air systems: a critical literature review, Build. Environ. 111 (2017) 123–131, doi:10.1016/j.buildenv.2016.10.020.

[7] K. Carbonnier, C. Higgins, F. Bauman, C. Karmann, P. Raftery, S. Schiavon, L.T. Graham, Energy use, occupant surveys and case study summary: radiant cooling and heating in commercial buildings - eScholarship, 2017 accessed December 5, 2017. https://escholarship.org/uc/item/3cj9n3n4#main.

[8] NBI, Getting to Zero Database, New Buildings Institute, 2018 accessed March 23, 2018. https://newbuildings.org/resource/getting-to-zero-database/.

[9] J. Babiak, B. Olesen, D. Petras, REHVA Guidebook No. 7: Low temperature Heating and High Temperature Cooling, Federation of European Heating and Air–Conditioning Associations, Brussels, Belgium, 2009.

[10] C. Duarte, P. Raftery, S. Schiavon, F. Bauman, How high can you go? Determining the highest supply water temperature for high thermal mass radiant cooling systems in California, (2018) 6.

[11] D.O. Rijksen, C.J. Wisse, A.W.M. van Schijndel, Reducing peak requirements for cooling by using thermally activated building systems, Energy Build. 42 (2010) 298–304, doi:10.1016/j.enbuild.2009.09.007.

[12] B. Lehmann, V. Dorer, M. Koschenz, Application range of thermally activated building systems tabs, Energy Build. 39 (2007) 593–598, doi:10.1016/j.enbuild.2006.09.009.

[13] B. Ning, S. Schiavon, F.S. Bauman, A novel classification scheme for design and control of radiant system based on thermal response time, Energy Build. 137 (2017) 38–45, doi:10.1016/j.enbuild.2016.12.013.

[14] M. Sourbron, R. De Herdt, T. Van Reet, W. Van Passel, M. Baelmans, L. Helsen, Efficiently produced heat and cold is squandered by inappropriate control strategies: a case study, Energy Build. 41 (2009) 1091–1098, doi:10.1016/j.enbuild.2009.05.015.

[15] M. Sourbron, L. Helsen, Sensitivity analysis of feedback control for concrete core activation and impact on installed thermal production power, J. Build. Perform. Simul. 7 (2014) 309–325, doi:10.1080/19401493.2013.824028.

[16] P. Raftery, C. Duarte, S. Schiavon, F. Bauman, A new control strategy for high thermal mass radiant systems, in: Proc. Build. Simul. 2017, 2017.

[17] G. Paliaga, F. Farahmand, P. Raftery, J. Woolley, TABS radiant cooling design & control in North America: results from expert interviews, EScholarship (2017). http://escholarship.org/uc/item/0w62k5pq. accessed July 23, 2017.

[18] P. Weitzmann, Modelling building integrated heating and cooling systems, 2004 accessed November 30, 2016. http://www.forskningsdatabasen.dk/en/catalog/2185770864 .

[19] J. Romaní, A. de Gracia, L.F. Cabeza, Simulation and control of thermally activated building systems (TABS), Energy Build. 127 (2016) 22–42, doi:10.1016/j.enbuild.2016.05.057.

[20] E. Berger, The Hidden daytime price of electricity, ASHRAE J. 57 (2015) 64.

[21] S. Bahrami, M.H. Amini, M. Shafie-khah, J.P.S. Catalao, A decentralized electricity market scheme enabling demand response deployment, IEEE Trans. Power Syst. PP (2017) 1–1, doi:10.1109/TPWRS.2017.2771279.

[22] A. Afram, F. Janabi-Sharifi, Theory and applications of HVAC control systems – a review of model predictive control (MPC), Build. Environ. 72 (2014) 343–355, doi:10.1016/j.buildenv.2013.11.016.

[23] Y. Ma, A. Kelman, A. Daly, F. Borrelli, Predictive control for energy efficient buildings with thermal storage: modeling, stimulation, and experiments, IEEE Control Syst. 32 (2012) 44–64, doi:10.1109/MCS.2011.2172532.

[24] T. Zakula, P.R. Armstrong, L. Norford, Modeling environment for model predictive control of buildings, Energy Build. 85 (2014) 549–559, doi:10.1016/j.enbuild.2014.09.039.

[25] J. Hu, P. Karava, Model predictive control strategies for buildings with mixed-mode cooling, Build. Environ. 71 (2014) 233–244, doi:10.1016/j.buildenv.2013.09.005.

[26] F. Oldewurtel, A. Parisio, C.N. Jones, D. Gyalistras, M. Gwerder, V. Stauch, B. Lehmann, M. Morari, Use of model predictive control and weather forecasts for energy efficient building climate control, Energy Build. 45 (2012) 15–27, doi:10.1016/j.enbuild.2011.09.022.

[27] F. Oldewurtel, D. Sturzenegger, M. Morari, Importance of occupancy information for building climate control, Appl. Energy. 101 (2013) 521–532, doi:10.1016/j.apenergy.2012.06.014.

[28] G.P. Henze, C. Felsmann, G. Knabe, Evaluation of optimal control for active and passive building thermal storage, Int. J. Therm. Sci. 43 (2004) 173–183, doi:10.1016/j.ijthermalsci.2003.06.001.

[29] D.Q. Mayne, J.B. Rawlings, C.V. Rao, P.O.M. Scokaert, Constrained model predictive control: stability and optimality, Automatica 36 (2000) 789–814, doi:10.1016/S0005-1098(99)00214-9.

[30] J. (Dove) Feng, F. Chuang, F. Borrelli, F. Bauman, Model predictive control of radiant slab systems with evaporative cooling sources, Energy Build. 87 (2015) 199–210, doi:10.1016/j.enbuild.2014.11.037.

[31] F. Chuang, Fast predictive control of networked energy systems, EScholarship (2015). http://escholarship.org/uc/item/4p87x9tc. accessed October 16, 2017.

[32] F. Borrelli, A. Bemporad, M. Morari, Predictive Control for Linear and Hybrid Systems, Cambridge University Press, 2017.

[33] LBNL, FLEXLAB: The world's most advanced building efficiency test bed, 2016 accessed October 30, 2017. https://flexlab.lbl.gov/sites/all/files/featured/LBNL_HANDOUT_v16-download.pdf .

[34] M.A. Humphreys, The optimum diameter of a globe thermometer for use indoors, Annu. Occup. Hyg. 20 (1977) 135–140, doi:10.1093/annhyg/20.2.135.

[35] S. Dawson-Haggerty, X. Jiang, G. Tolle, J. Ortiz, D. Culler, sMAP - a simple measurement and actuation profile for physical information, in: Proceedings of the Eighth ACM Conference on Embedded Networked Sensor Systems (SenSys '10), November 2010.

[36] ASHRAE, ASHRAE Guideline 14-2014: Measurement of Energy, Demand, and Water Savings, Atlanta, GA USA.

[37] NOAA, National Oceanic and Atmospheric Administration (2018). www.weather.gov.